University of Wollongong

Research Online

Faculty of Engineering and Information Sciences - Papers: Part A

Faculty of Engineering and Information Sciences

31-12-2012

Synthesis of Mn3O4-encapsulated graphene sheet nanocomposites via a facile, fast microwave hydrothermal method and their supercapacitive behaviour

Li Li
University of Wollongong, li@uow.edu.au

Kuok Hau Seng
University of Wollongong, kseng@uow.edu.au

Zhixin Chen
University of Wollongong, zchen@uow.edu.au

Hua-Kun Liu
University of Wollongong, hua@uow.edu.au

Ivan P. Nevirkovets
University of Wollongong, ivann@uow.edu.au

See next page for additional authors

Follow this and additional works at: https://ro.uow.edu.au/eispapers

 Part of the Engineering Commons, and the Science and Technology Studies Commons

Recommended Citation

Li, Li; Seng, Kuok Hau; Chen, Zhixin; Liu, Hua-Kun; Nevirkovets, Ivan P.; and Guo, Zaiping, "Synthesis of Mn3O4-encapsulated graphene sheet nanocomposites via a facile, fast microwave hydrothermal method and their supercapacitive behaviour" (2012). *Faculty of Engineering and Information Sciences - Papers: Part A*. 497.
https://ro.uow.edu.au/eispapers/497

Research Online is the open access institutional repository for the University of Wollongong. For further information contact the UOW Library: research-pubs@uow.edu.au

Synthesis of Mn3O4-encapsulated graphene sheet nanocomposites via a facile, fast microwave hydrothermal method and their supercapacitive behaviour

Abstract

Well-crystallized Mn3O4-anchored reduced graphene oxide (rGO) nanocomposites have been successfully synthesized via a facile, effective, energy-saving, and scalable microwave hydrothermal technique for potential application as supercapacitor material. Integrating these nanostructures resulted in a strong synergistic effect between the two materials, consequently leading to a hybrid composite with higher specific capacitance compared to the bare Mn3O4 nanoparticles. The results from different sorts of characterization indicate that the Mn3O4 particles were deposited and anchored on graphene sheets. The capacitance value of the rGO(31.6%)–Mn3O4 nanocomposite reached 153 F/g, much higher than that of the bare Mn3O4 (87 F/g) at a scan rate of 5 mV/s in the potential range from −0.1 V to 0.8 V. More importantly, a 200% increase in capacitance was observed for the nanocomposite with cycling at 10 mV/s due to electrochemical activation and the oxidization of Mn(II,III) to Mn(IV) during cycling, as verified by Xray photoelectron spectroscopy. There is no observable capacitance fading up to 1000 cycles. The facile synthesis method and good electrochemical properties indicate that the nanocomposite could be an electrode candidate for supercapacitors.

Keywords

microwave, hydrothermal, method, their, supercapacitive, behaviour, synthesis, mn3o4, encapsulated, graphene, sheet, nanocomposites, via, facile, fast

Disciplines

Engineering | Science and Technology Studies

Publication Details

Li, L., Seng, K., Chen, Z., Liu, H., Nevirkovets, I. P. & Guo, Z. (2013). Synthesis of Mn3O4-encapsulated graphene sheet nanocomposites via a facile, fast microwave hydrothermal method and their supercapacitive behaviour. Electrochimica Acta, 87 801-808.

Authors

Li Li, Kuok Hau Seng, Zhixin Chen, Hua-Kun Liu, Ivan P. Nevirkovets, and Zaiping Guo

This journal article is available at Research Online: https://ro.uow.edu.au/eispapers/497

Synthesis of Mn_3O_4-anchored graphene sheet nanocomposites via a facile, fast microwave hydrothermal method and their supercapacitive behavior

Li Li,[a] Kuok Hau Seng, [a] Huakun Liu [a], Ivan P. Nevirkovets,[a] Zaiping Guo [*,a, b]

a Institute for Superconducting and Electronics Materials, University of Wollongong, Wollongong 2519, Australia

b School of Mechanical, Materials, and Mechatronic Engineering, University of Wollongong, Wollongong 2522, Australia

Abstract: Well-crystallized Mn_3O_4-anchored reduced graphene oxide (rGO) nanocomposites have been successfully synthesized via a facile, effective, energy-saving, and scalable microwave hydrothermal technique for potential application as supercapacitor material. Integrating these nanostructures resulted in a strong synergistic effect between the two materials, consequently leading to a hybrid composite with higher specific capacitance compared to the bare Mn_3O_4 nanoparticles. The results from different sorts of characterization indicate that the Mn_3O_4

[*] Corresponding author: Institute for Superconducting and Electronics Materials, University of Wollongong, Squires Way, Fairy Meadow, Wollongong 2519, NSW, Australia.Tel.:+61 2 4221 5225, Fax: +61 2 4221 5731, *E-mail address*: zguo@uow.edu.au .

particles were deposited and anchored on graphene sheets. The capacitance value of the rGO(31.6%)-Mn_3O_4 nanocomposite reached 153 F/g, much higher than that of the bare Mn_3O_4 (87 F/g) at a scan rate of 5 mV/s in the potential range from -0.1 V to 0.8 V. More importantly, a 200% increase in capacitance was observed for the nanocomposite with cycling at 10 mV/s due to electrochemical activation and the oxidization of Mn(II,III) to Mn(IV) during cycling, as verified by X-ray photoelectron spectroscopy. There is no observable capacitance fading up to 1000 cycles. The facile synthesis method and good electrochemical properties indicate that the nanocomposite could be an electrode candidate for supercapacitors.

Keywords: microwave hydrothermal, graphene, Mn_3O_4, nanocomposite, supercapacitor

1. Introduction

In order to meet the need for high power energy storage systems, the electrochemical capacitor (EC) [1], also known as the ultracapacitor or supercapacitor, is an attractive energy storage device that is arousing much attention at present. It is well known that an electrochemical capacitor can be fully charged or discharged in seconds, which delivers a much higher power density (10 kW/kg) over a shorter time compared to batteries [2,3]. Its energy density (about 5 Wh/kg), however, is significantly lower than for lithium ion batteries (150-250 Wh/kg). Therefore, the supercapacitor can play a significant role in complementing lithium ion batteries in various energy storage applications, such as in emergency power supplies and peak power assistance in electric vehicles.

Based on the charge storage mechanism and the active materials used, supercapacitors can be classified into two types. The first group only involves physical adsorption of ions, without any chemical reactions, and such capacitors are called electric double-layer capacitors (EDLC), the

typical electrode materials of which are carbon-based active materials with high surface area and low cost [4]. For the second group, the capacitors are termed pseudocapacitors or redox supercapacitors, which can rapidly transfer faradic charges between the electrolyte and electrode at the surface or near-surface of the active materials for charge storage [5]. Transition metal oxides, conducting polymers [6,7], and carbon composites [3,8-11], including graphene based composites [12-16], can be used in this class and have been extensively studied in past decades. Among these materials, the most widely studied metal oxide is hydrous ruthenium oxide (RuO_xH_y or $RuO_2 \bullet xH_2O$) due to its high electrical conductivity, on the order of 10^5 S/cm (at room temperature), and its ultra-high theoretical capacitance (~2000 F/g) in a wide potential window of 1.4 V, as well as its excellent chemical stability [17]. However, owing to the rarity of Ru, Ru-based aqueous electrochemical capacitors are very expensive, limiting any wide commercial applications. Manganese oxides are considered as one of the most cost-effective transition metal oxide materials for the next generation of supercapacitors due to their low cost, environmentally friendly nature, and high theoretical specific capacitance [18a]. There are only a few articles, however, that have reported Mn_3O_4 as electrode material for pseudosupercapacitors so far, due to its intrinsic insulating properties (~10^{-7}-10^{-8} S/cm). Cui et al. [18b] reported that the specific capacitance for MWCNT/Mn_3O_4 with high mass loading of 10 mg/cm^2 was 143 F/g at the scan rate of 2 mV/s, and 81% of capacitance can be retained after 100 cycles. Fang et al. [18c] found that there was 100% retention of the specific capacitance of Mn_3O_4 powders as supercapacitive electrode after 400 cycles, based on an initial capacitance of 148 F/g, but the mass loading was very low, only 0.01g/cm^2, so the poor electronic conductivity limits the performance of Mn_3O_4 as supercapacitive active material. In order to improve the capacitive performance of Mn_3O_4 electrodes, a promising approach is to construct composite electrodes with Mn_3O_4 nanostructures embedded in a highly conductive porous matrix. Robust and flexible two-dimensional (2-D)

graphene sheets (GS) are an excellent matrix material to encapsulate Mn_3O_4. This is due to graphene's high conductivity, large surface area, flexibility, and chemical stability [19-23].

Herein, we have fabricated well-organized graphene sheets with Mn_3O_4 to form nanocomposites via a facile, fast, and scalable microwave hydrothermal technique. The microwave hydrothermal method, compared with the traditional hydrothermal method, can increase the kinetics of crystallization by promoting rapid nucleation and growth, as well as offering great possibilities for large-scale batch reactions; therefore, it can achieve large energy savings. In addition, in these composites, the Mn_3O_4 nanoparticles were deposited on and further anchored on the highly conductive graphene sheets, which will not only function as an ionic and electronic transport medium in the electrode during the cycling, but could prevent the possible detachment of Mn_3O_4 from the graphene sheets during cycling. The high specific surface area also has benefits for the accommodation of electric double layer capacitance and Mn_3O_4 deposition, so that the as-prepared rGO-Mn_3O_4 nanocomposites can preserve high electrical conductivity throughout the whole electrode, which leads to higher capacitance in the supercapacitor compared to the bare Mn_3O_4. Furthermore, we also observed that there was a 200% increase in capacitance for the nanocomposite with cycling at 10 mV/s as a result of electrochemical activation and oxidization of Mn(II,III) to Mn(IV) in the electrolyte during cycling, which has been proved by X-ray photoelectron spectroscopy (XPS) analysis in this work, and the Mn(IV) is further deposited as MnO_2, which will increase the capacitance due to its higher electric conductivity. A similar phenomenon was observed in the work reported by Komaba et al. [43], however, their work did not pay much attention to the intrinsic factor of the oxidization of Mn(II,III) [24].

2. Experimental section

2.1 Synthesis of the rGO-Mn_3O_4 nanocomposites

Graphite oxide (GO) was prepared using a modified Hummers' method as described elsewhere [25]. In a typical preparation of rGO-Mn_3O_4 nanocomposite (composite 2), 10 mL of manganese acetate (0.2 mol/L) aqueous solution was added into 100 mL of as-prepared GO (0.5 mg/mL) dispersion under vigorous magnetic stirring for 4 hours. 2 mL of NaOH (2 mol/L) aqueous solution was added dropwise to the above mixture, followed by stirring overnight. Subsequently, 0.23 mL anhydrous hydrazine was added to the above solution with stirring for 0.5 h, and then the solution was diluted by the addition of 100 mL de-ionized water. Finally, 20 mL of this brown solution was transferred to a Teflon-lined autoclave and then was irradiated in a Milestone Microsynth Microwave Labstation (Germany) for 30 min at 150°C. The formation of Mn_3O_4 is represented by the following Equations (1) and (2) [26]:

$$Mn^{2+} + 2OH^- \longrightarrow Mn(OH)_2 \qquad (1)$$

$$3Mn(OH)_2 + (1/2)O_2 \longrightarrow Mn_3O_4 + 3H_2O \qquad (2)$$

After the reaction, the precipitate was collected with a centrifuge and rinsed with de-ionized water and ethanol three times, respectively. Afterwards, the obtained powders were dried at 60°C overnight in a vacuum oven. For comparison, nanocomposites with other ratios of Mn_3O_4 to rGO (composite 1, composite 3) were also prepared by the same experimental procedure, except that the amount of GO and anhydrous hydrazine were 50 mL and 0.19 mL, and 150 mL and 0.27 mL, respectively. Bare Mn_3O_4 nanoparticles were also synthesized by the same procedure but without the addition of GO. Pure rGO was synthesized according to a report by Li [25]. The content of rGO in the composites was estimated by using thermogravimetric analysis (TGA). It was found that the weight percent of rGO in the three rGO-Mn_3O_4 nanocomposites was about 18.8 wt.%, 31.6 wt.%, and 45 wt.%, respectively (Figure S1 in the Supporting Information).

2.2 Materials characterization.

The phase structure of the as-prepared products was characterized by X-ray diffraction (XRD; MMA GBC with Cu K radiation) and Raman spectroscopy (Jobin Yvon HR800). The morphology and size of the as-obtained products were investigated using field-emission scanning electron microscopy (FESEM; JEOL-7500, 2 keV) and transmission electron microscopy (TEM; JEOL-2010, 200 keV). Thermogravimetric analysis was conducted on a TA 2000 Thermo-analyzer. The elemental composition was characterized by X-ray photoelectron spectroscopy (XPS; PHOIBOS 100 hemispherical analyser, SPECS GmbH), and the excitation was Al K radiation at 10 kV (100 W). The survey spectra were collected with pass energy of 69 eV, and the particular lines with pass energy of 20 eV.

The working electrodes were prepared by mixing 80 wt.% rGO-Mn_3O_4 nanocomposite powder and 10 wt% carbon black, along with 10 wt% polyvinylidene difluoride (PVdF), in the presence of N-methyl pyrrolidinone (NMP), and this slurry was pasted on stainless steel mesh and then heat treated at 80°C under vacuum overnight. Beaker-type three-electrode cells were assembled with a working electrode, a counter electrode (platinum foil), and a reference electrode (saturated calomel electrode (SCE)) in 1 M Na_2SO_4 electrolyte. Cyclic voltammetry (CV) and galvanostatic charge-discharge measurements were performed over the potential range from - 0.1 V to 0.8 V at various scan rates (5 to 50 mV/s) and different current densities (0.2 A/g - 5 A/g) on a VMP-3 electrochemical workstation. For comparison, the electrochemical performance of the bare Mn_3O_4 nanoparticles and pure rGO were also investigated under the same conditions.

3. Results and discussion

Figure 1 presents the X-ray diffraction (XRD) patterns of the graphene oxide (GO), reduced graphene oxide (rGO), bare Mn_3O_4 nanoparticles, and rGO(31.6%)-Mn_3O_4 nanocomposite. The diffraction peak at 9.7° is indexed to GO, and the appearance of the (002) diffraction line at 23.4° for rGO [27] gives evidence that the graphite oxide was reduced to graphene during the microwave hydrothermal process. Meanwhile, it can also be observed that the peaks of graphene become broadened after reduction, which is a typical pattern for amorphous carbon structure [28], revealing that the stacking of graphene sheets is substantially disordered.

The peaks assigned in Figure 1 correspond to the Mn_3O_4, which has a tetragonal spinel structure with space group I41/amd (JCPDS card: 24-0734), and they also match well with previous report in the literature [29]. No other crystalline impurity phases can be observed.

In addition, the presence of both rGO and Mn_3O_4 phases is indicated by typical peaks in the Raman spectra (Figure 2). Figure 2 contains typical Raman spectra of GO, bare Mn_3O_4 nanoparticles, and rGO(31.6%)-Mn_3O_4 nanocomposite. For the GO and rGO(31.6%)-Mn_3O_4 nanocomposite samples, the G band (1604 cm^{-1}) arises from the zone centre E_{2g} mode, corresponding to ordered sp^2 bonded carbon, whereas the D band (1330 cm^{-1}) is ascribed to edges or disordered layers. The intensity ratio of the D to the G band (I_D/I_G) provides a sensitive measure of the disorder and the crystallite size of the graphitic layers [30]. In comparison, the intensity ratio I_D/I_G for GO (1.08) is lower than that of the rGO(31.6%)-Mn_3O_4 composite (1.31), which is due to the presence of unrepaired defects that have remained after the removal of oxygen moieties [31], suggesting that the reduction of exfoliated GO leads to smaller and more disordered layers, as well as dramatically decreasing the number of stacked graphene layers [32]. In addition, minor peaks at 317, 374, and 475 cm^{-1}, as well as a dominant peak at 652 cm^{-1} in the rGO-Mn_3O_4 nanocomposite, can be ascribed to specific vibrations of pure crystalline Mn_3O_4 [33, 34], which are substantially coincident with those of the bare Mn_3O_4. The Raman spectrum of

rGO-Mn_3O_4 nanocomposite is actually that of a combination of pure reduced graphene oxide and bare Mn_3O_4. This implies that Mn_3O_4 and rGO are in their own pristine structures, and no chemical reactions have occurred between them during the in situ hydrothermal synthesis process.

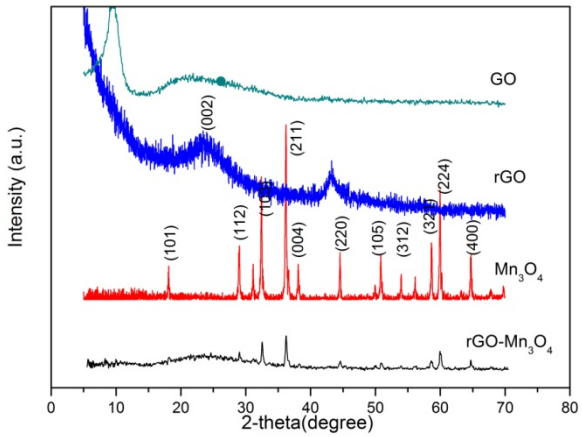

Figure 1. X-ray diffraction patterns of (a) GO, (b) rGO, (c) bare Mn_3O_4 nanoparticles, and (d) as-prepared rGO(31.6%)-Mn_3O_4 nanocomposite.

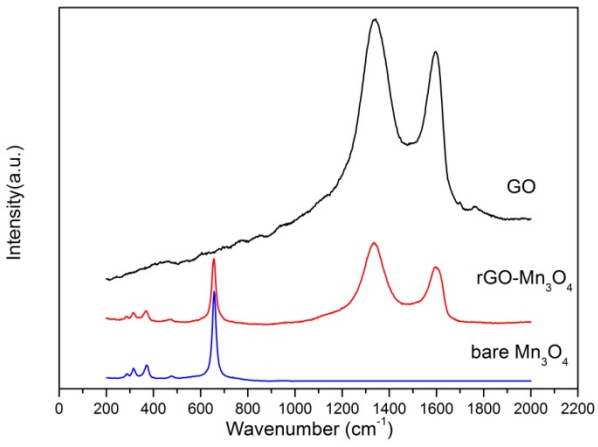

Figure 2. Raman spectra of GO, rGO(31.6%)-Mn_3O_4 nanocomposite, and bare Mn_3O_4 nanoparticles.

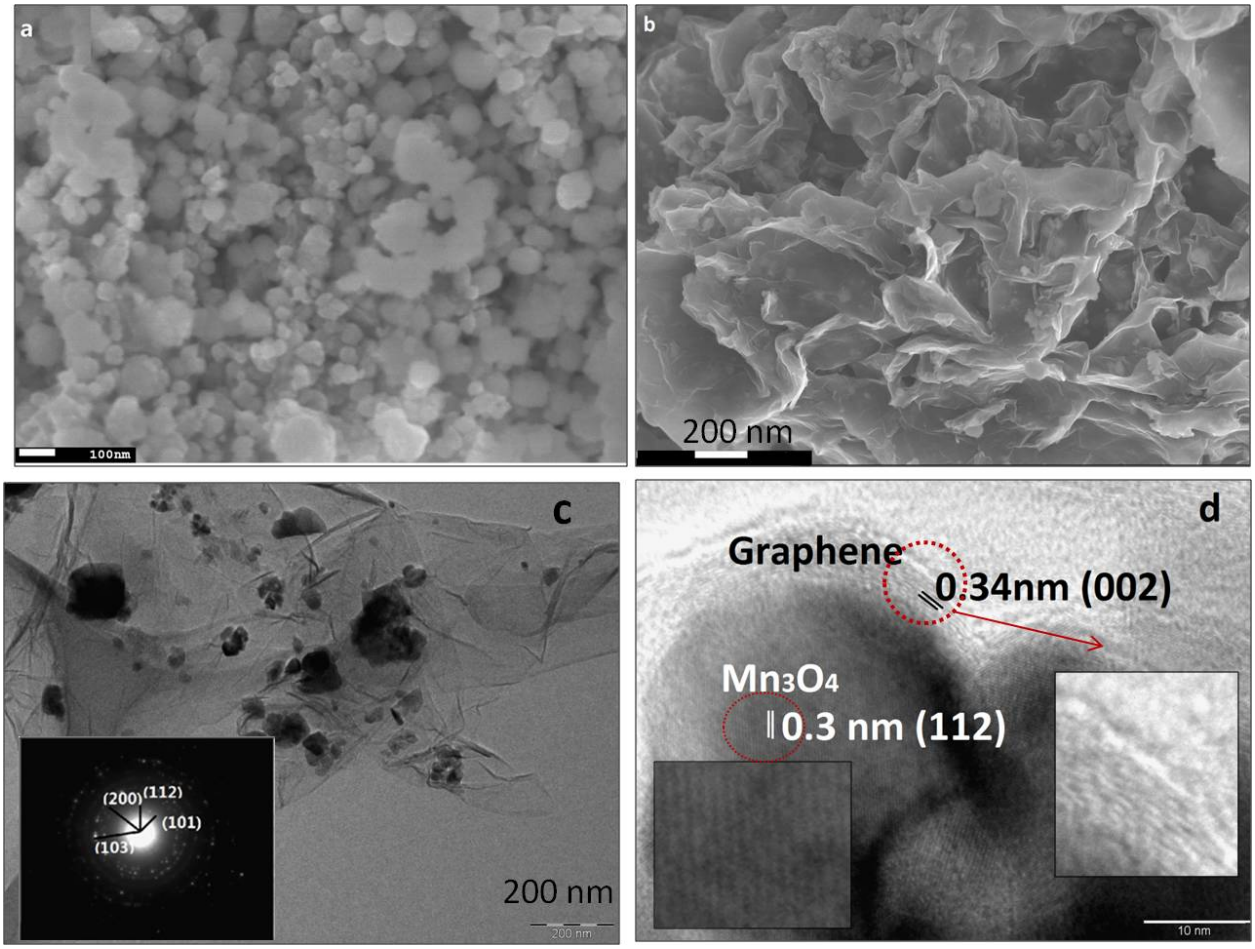

Figure 3. FESEM images of (a) bare Mn_3O_4 nanoparticles, and (b) rGO(31.6%)-Mn_3O_4 nanocomposite. TEM images of rGO(31.6%)-Mn_3O_4 nanocomposite: (c) large-area image and associated selected-area electron diffraction (SAED) pattern (inset), (d) high-resolution TEM image of Mn_3O_4 particle in [112] orientation embedded in graphene sheets.

To investigate the morphologies of the products, field-emission scanning electron microscope (FESEM) images were collected for the bare Mn_3O_4 nanoparticles and the rGO(31.6%)-Mn_3O_4 nanocomposite, as shown in Figure 3. The morphology of the bare Mn_3O_4 nanoparticles,

prepared by the same procedure as for the rGO-Mn_3O_4 nanocomposite, is spherical, but the nanoparticles are severely aggregated, giving rise to bigger particle sizes in the range of 40-100 nm (Figure 3(a)). In comparison, we can observe that the size of the Mn_3O_4 nanoparticles is dramatically decreased to around 20 nm when they are prepared in situ with GO via the microwave hydrothermal method, as shown in Figure 3(b), due to the intimate attachment to the flexible graphene sheets, which limits the growth and agglomeration of the crystalline Mn_3O_4 particles.

The transmission electron microscope (TEM) images in Figure 3(c) and (d) reveal that the Mn_3O_4 nanoparticles are distributed on the surfaces of the graphene nanosheets in the form of either single particles or small particle clusters, and the nature of the Mn_3O_4 particles shown in Figure 3(c) was further confirmed by selected area electron diffraction (SAED) patterns (inset of Figure 3(c)). The visible diffraction rings can be indexed to Hausmannite Mn_3O_4 phase, which is consistent with the XRD patterns. The high-resolution TEM image (Figure 3(d)) indicates that there are multiple overlapping layers near the edges of the Mn_3O_4 particles, whereas the *d*-spacing of the (002) graphene planes is 0.34 nm, almost equal to the value of pristine graphene. The Mn_3O_4 particles are anchored on the graphene sheets, and their crystal lattice fringes with *d*-spacing of 0.3 nm can be assigned to the (112) planes of tetragonal Mn_3O_4. Based on the FESEM and TEM images, it could be confirmed that there is an intimate interaction between the Mn_3O_4 particles and the graphene sheets, and this combination could be an ideal way to construct composite materials which not only take advantage of the graphene sheets to enable fast electron transport from the graphene matrix to the Mn_3O_4 nanoparticles, but also retain this benefit for a longer time, guaranteeing the enhancement of the cycling performance.

The specific capacitance of the as prepared samples was estimated from the cyclic voltammograms (CVs) by integrating the area under the current-potential curve and then

dividing by the sweep rate ( ), the mass of the film (*m*), and the potential window, according to Equation (3) [35]:

$$C = \frac{1}{mv(V_a - V_c)} \int_{V_a}^{V_c} I(V)dV \quad (3)$$

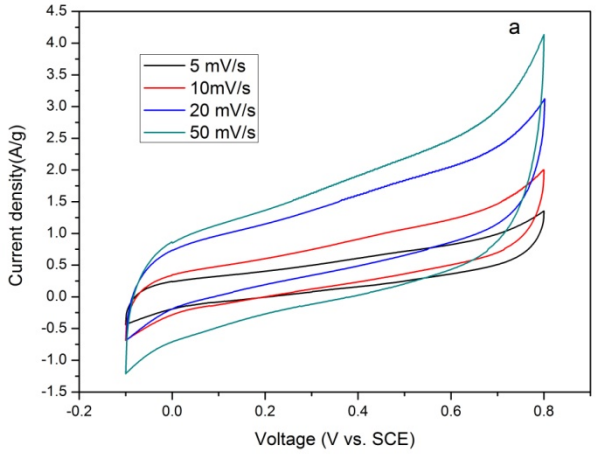

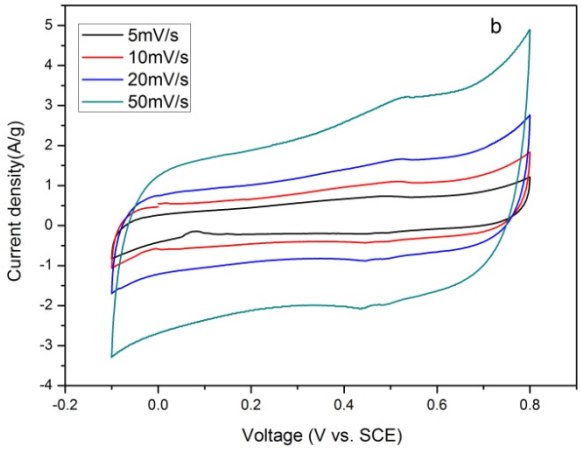

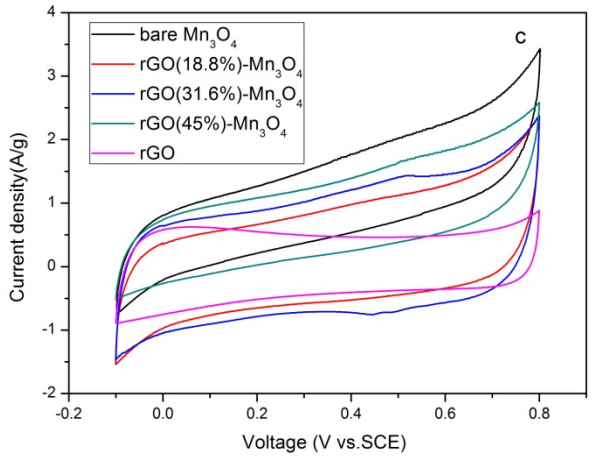
bare Mn_3O_4
rGO(18.8%)-Mn_3O_4
rGO(31.6%)-Mn_3O_4
rGO(45%)-Mn_3O_4
rGO
c
Current density(A/g)
Voltage (V vs.SCE)

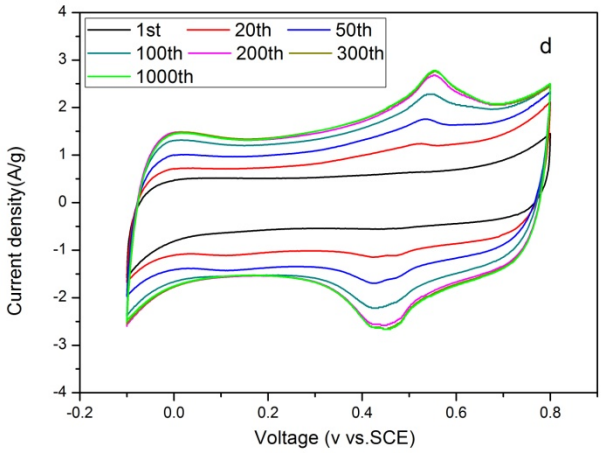
1st
20th
50th
100th
200th
300th
1000th
d
Current density(A/g)
Voltage (v vs.SCE)

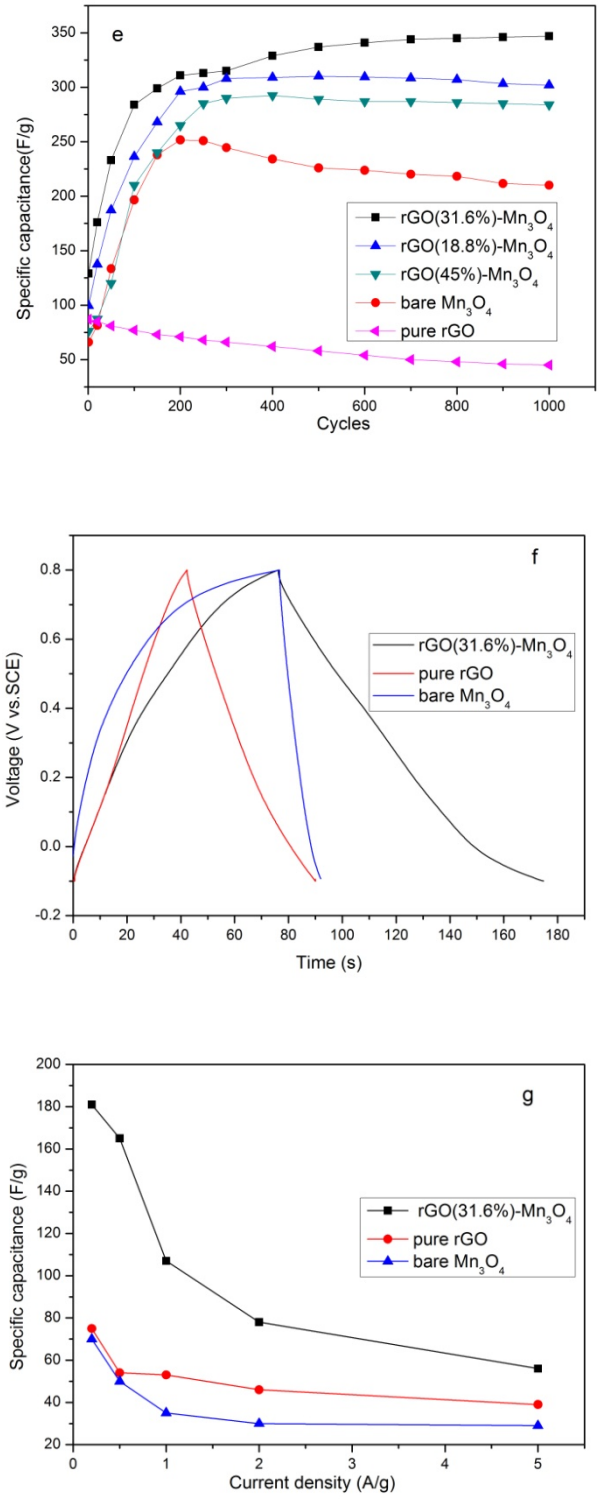

Figure 4. Cyclic voltammograms of electrodes made from (a) bare Mn_3O_4 nanoparticles at

different scan rates, (b) rGO(31.6%)-Mn_3O_4 nanocomposite at different scan rates, (c) bare Mn_3O_4 nanoparticles, pure rGO, and rGO(18.8%, 31.6%, 45%)-Mn_3O_4 nanocomposites at the scan rate of 20 mV/s, (d) rGO(31.6%)-Mn_3O_4 composite in typical selected cycles at the scan rate of 10 mV/s, and (e) cycling stability of rGO(18.8%, 31.6%, 45%)-Mn_3O_4 nanocomposites, bare Mn_3O_4 nanoparticles, and pure rGO electrodes at the scan rate of 10 mV/s. (f) Galvanostatic charge–discharge curves of bare Mn_3O_4 nanoparticles and rGO(31.6%)-Mn_3O_4 nanocomposite at current density of 1 A/g, (g) Specific capacitance calculated from galvanostatic charge–discharge curves at different current densities of bare Mn_3O_4 nanoparticles and rGO(31.6%)-Mn_3O_4 nanocomposite. All cyclic voltammograms and galvanostatic charge-discharge profiles were measured in 1 M Na_2SO_4 electrolyte in the voltage range from -0.1 V to 0.8 V.

Figure 4(a) and (b) compare the cyclic voltammogram profile of the bare Mn_3O_4 nanoparticle electrode with that of the rGO(31.6%)-Mn_3O_4 nanocomposite electrode at different scan rates in 1 M Na_2SO_4 electrolyte. The anodic and cathodic potential limits were set to 0.8 V and - 0.1 V vs. SCE, due to the irreversible reactions beyond these two limits of the potential window in the hydrous electrolyte [36]. The CV profiles of composites 1 and 3, and of pure rGO are shown in Figure S2(a-c).

Obviously, the rGO(31.6%)-Mn_3O_4 nanocomposite electrode presents the largest integrated area compared to the bare Mn_3O_4 nanoparticle electrode, the pure rGO, and the other two nanocomposite electrodes, as shown in Figure 4(c), and all of these nanocomposite and bare Mn_3O_4 electrodes exhibit the typical characteristics of pseudocapacitive behavior. The specific capacitance of the bare Mn_3O_4 nanoparticles and the rGO(31.6%)-Mn_3O_4 nanocomposite was calculated to be 87 F/g and 153 F/g, respectively, at 5 mV/s according to Equation (3), as shown

in Table 1, indicating that the capacitance of the nanocomposite has been significantly increased due to the addition of GO. The enhancement in capacitance can be ascribed to the large specific surface area of the graphene in the nanocomposite material, which favours charge storage and ion transfer, and there is also a significant charge transfer from the graphene layer to the Mn_3O_4(001) surface in the ground electronic state, based on our previous theoretical computations [37], which can considerably enhance the electronic conductivity of the whole nanocomposite.

An increase in the anodic and cathodic currents of the rGO(31.6%)-Mn_3O_4 nanocomposite with cycling is also clearly observed in the CV curves over the whole potential range, with cycling at the scan rate of 10 mV/s, particularly before 200 cycles. The current response in the CV become stable after around 300 cycles (Figure 4(d)). As shown in Figure 4(e), the specific capacitance of rGO(31.6%)-Mn_3O_4 reaches a value of approximately 315 F/g at the 300th cycle, much higher than that reported in previous work [38]. In particular, after 300 cycles, the specific capacitance slightly increases up to 1000 cycles. The shape of the CV profiles, as shown in Figure 4(d), become more rectangular, and the cathodic peak at around 0.5 V and the anodic peak at 0.4 V generally become stronger, while the peaks shift toward higher potential with cycling, which could be attributed to both the electrochemical activation of the rGO(31.6%)-Mn_3O_4 electrode and the oxidization of the low valence state of Mn ions [39,44]. In comparison, a similar trend towards increasing capacitance can be observed in the bare Mn_3O_4 nanoparticles, as well as the rGO(18.8%)-Mn_3O_4 and rGO(45%)-Mn_3O_4 nanocomposites, but the specific capacitance for pure rGO decreased gradually to 45 F/g after 1000 cycles in Figure 4(e). The specific capacitance of the bare Mn_3O_4 nanoparticles experienced a slight decay after 200 cycles after an increase from 66 F/g in the initial cycle to 251 F/g at the 200th cycle, while the specific capacitance values for the nanocomposites (rGO(18.8%, 45%)-Mn_3O_4) could remain stable up to

1000 cycles, which further indicates that the graphene sheets in this composite play a significant role in terms of ensuring high conductivity and cycling stability through intimate interaction with the Mn_3O_4 nanoparticles.

Galvanostatic charge–discharge (CD) measurements performed on the three electrodes in a potential window from -0.1 to 0.8 V provide a complementary measurement of the capacitance. Figure 4(f) shows the charge–discharge profiles of the bare Mn_3O_4, pure rGO, and rGO(31.6%)-Mn_3O_4 nanocomposite electrodes at the current density of 1 A/g. The rGO electrode presents linear charge and discharge profiles, indicating purely capacitive behavior, however, for bare Mn_3O_4 and the nanocomposite, the charge curve is almost symmetric with its corresponding discharge counterpart, with a small internal resistance (IR) drop, indicating the pseudocapacitive contribution, along with the double layer contribution. The specific capacitance was calculated using Equation (4):

$$C = \frac{i \times \Delta t}{m \times \Delta E} \quad (4)$$

where i is the discharge current, Δt, the discharge time, m, the mass of the active material and ΔE, the potential window. The specific capacitances calculated from the charge–discharge profiles in Figure 4(f) were 35, 53, and 107 F/g for bare Mn_3O_4, rGO, and rGO(31.6%)-Mn_3O_4 nanocomposite, respectively. Figure 4(g) shows the variation in the specific capacitance with current density. A sharp decrease in specific capacitance is observed at low current densities. The specific capacitance of bare Mn_3O_4 was 70, 50, 35, 30, and 29 F/g at 0.2, 0.5, 1, 2, and 5 A/g, respectively, and the specific capacitance for pure rGO was 75, 54, 53, 46, and 39 F/g at 0.2, 0.5, 1, 2, and 5 A/g. In contrast, the specific capacitance for the rGO(31.6%)-Mn_3O_4 nanocomposite was 181, 165, 107, 78, and 56 F/g at 0.2, 0.5, 1, 2, and 5 A/g. The higher capacitance of the

composite can be attributed to the improvement in conductivity in the presence of GO. The results are in agreement with those calculated using cyclic voltammetry, where a synergistic effect between the rGO and Mn_3O_4 is observed.

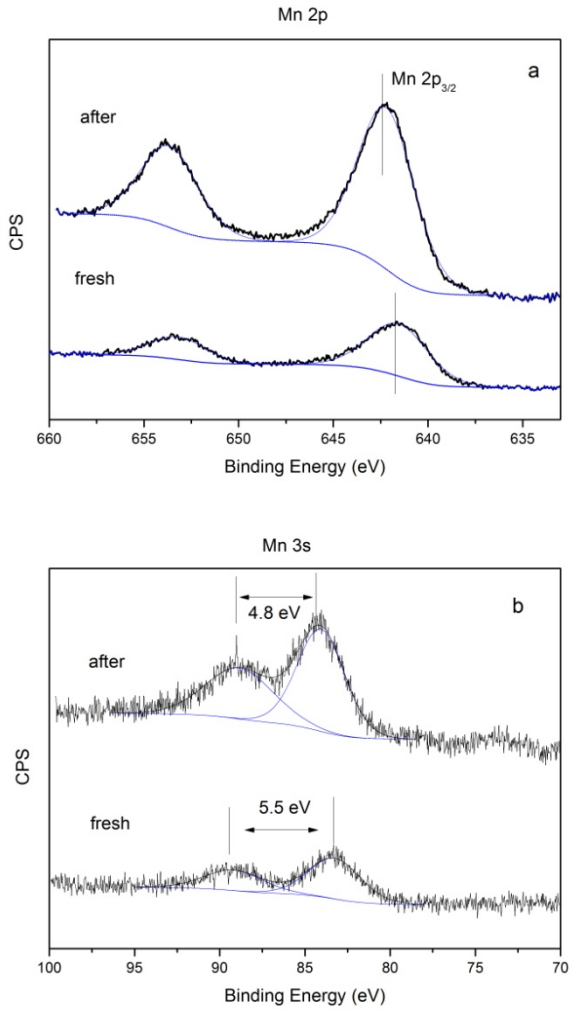

Figure 5. XPS spectra of the fresh electrode and the electrode after 1000 cycles for rGO(31.6%)-Mn_3O_4 nanocomposite in (a) the Mn 2p and (b) the Mn 3s region. Mixed Gaussian and Lorentzian component peaks are also exhibited in the spectra.

In order to confirm the factors behind the enhanced pseudocapacitive properties observed during cycling, X-ray photoelectron spectroscopy (XPS) was used to determine the oxidation

state of the fresh rGO(31.6%)-Mn_3O_4 nanocomposite and that of the same electrode after 1000 cycles. In Figure 5(a), the binding energy peaks of Mn $2p_{3/2}$ for the fresh electrode and the electrode after cycling are located at 641.5 eV and 642.2 eV, which are indexed to Mn_3O_4 and MnO_2, respectively, and they are also in good agreement with the literature [40], revealing that in the nanocomposite, Mn(II,III) ions may be oxidized to Mn(IV) after cycling.

Further evidence of the oxidation process can be seen from the multiplet splitting of the Mn 3s peaks in the core level spectra in Figure 5(b), which were further examined to assess the change in terms of the oxidation state of manganese between the fresh rGO(31.6%)-Mn_3O_4 nanocomposite electrode and the cycled electrode on the basis of the parallel spin coupling of the 3s electron with the 3d electron during the photoelectron ejection. The corresponding peak separation energy (E) is defined as the exchange interaction energy in Equation (5) [40-42]:

$$E = (2S+1)\ K\ [3s,3d] \qquad (5)$$

where S is the total spin of unpaired electrons in the 3s and 3d levels in the final states and K[3s, 3d] is the exchange integral between the 3s and 3d energy levels.

The energy separation between the two peaks is intrinsically related to the mean manganese oxidation state. Since a lower valence implies more electrons in the 3d orbital, more interaction can occur through photoelectron ejection. Consequently, the energy separation between the two components of the Mn 3s multiplet will increase at the lower valence. The inverse trend will be observed when the manganese valence increases. From Figure 5(b), we can observe that the splitting width of the electrode after cycling is 4.73 eV, smaller than before cycling (5.5 eV), indicating that the manganese oxidation state increased to Mn(IV), on the basis of an approximately linear relationship between the Mn 3s splitting width and the Mn oxidation state according to previous reports in the literature [40].

Based on XPS analysis and previous reports [39], it can be concluded that the as-prepared rGO(31.6%)-Mn_3O_4 was oxidized to Mn(IV) by electrochemical oxidation during cyclic voltammetry within the potential range from -0.1 to 0.8 V (vs. SCE) in 1 M Na_2SO_4 electrolyte. The electrochemically oxidized MnO_2 electrode showed better pseudocapacitive performance due to the enhanced electronic conductivity. Specifically, Mn_3O_4 has a spinel structure and is virtually an insulator, while MnO_2 is a semiconductor; therefore, the electrochemically oxidized MnO_2 exhibits higher electronic conductivity through the film matrix onto the current collector, which can exactly explain the interesting phenomenon of increasing capacitance with cycling described above.

Although a similar capacitance increase phenomenon has been observed and reported in quite a few papers on Mn_3O_4 as electrode material for supercapacitors [39,43], in some other reported work [44], the capacitance increase was not observed during cycling. The possible reason could be the partial detachment of Mn_3O_4 from the graphene sheets during cycling; therefore, the capacitance increase of the electrode due to the valence state change in the Mn ions and electrochemical activation will be sacrificed by the relatively lower utilization of Mn_3O_4, and the electrode will eventually show stable capacitance during cycling. It is well known that the electronic configuration of the 3d orbital in Mn(III) of Mn_3O_4 is expressed as t_{2g}^3–e_g^1, which indicates a typical Jahn-Teller ion having lower stabilization energy in the non-distorted octahedral environment. Mn(III) tends to be disproportionated into Mn(II) (t_{2g}^3–e_g^2) and Mn(IV) (t_{2g}^3), resulting in the release of Mn^{2+} ions into the electrolyte and also the phase conversion into MnO_2. It is very likely that Mn_3O_4 nanostructures detach from the graphene sheets when Mn^{2+} ions are dissolved into the electrolyte [43], and therefore, part of the Mn_3O_4 loses contact with the graphene sheets. In our work, Mn_3O_4 nanoparticles were still anchored on the graphene, even after 1000 cycles, as shown in Figure S3. It can be observed that the particle size of MnO_x after

cycling becomes smaller than in its fresh counterparts in Figure 3(c), and the smaller particles aggregate together as circled in Figure S3. In addition, the MnO_x particles become nearly amorphous due to repeated reduction/oxidation reactions. Hence, it appears that the electrochemical performance is significantly affected by the morphology and the distribution of the active materials.

4. Conclusions

In summary, we successfully synthesized Mn_3O_4-anchored graphene sheet nanocomposites from GO via a facile, effective, energy-saving, and scalable microwave hydrothermal technique. The Mn_3O_4 particles in the nanocomposites, directly growing on the surfaces of graphene sheets, interact with each other intimately, so that the rGO-Mn_3O_4 nanocomposites exhibit better performance in the pseudosupercapacitor than the bare Mn_3O_4 nanoparticles. The capacitance was raised from 87 F/g for the bare Mn_3O_4 to 153 F/g for the rGO(31.6%)-Mn_3O_4 nanocomposite in the presence of graphene oxide at the scan rate of 5 mV/s. Moreover, the capacitance for the rGO(31.6%)-Mn_3O_4 composite electrode reached 315 F/g at 300 cycles and remained stable up to 1000 cycles at the scan rate of 10 mV/s. The possible reasons for the capacitance increase during electrochemical cycling can be ascribed to: (1) Mn(II,III) was gradually oxidized to Mn(IV) in the electrolyte during cycling, which has been proved by XPS analysis in this paper. The Mn(IV) further deposited as MnO_2 will increase the capacitance due to its higher electric conductivity. (2) The ideal structure, in which the Mn_3O_4 nanoparticles were deposited on, and further attached intimately to graphene sheets, can enhance the electronic conductivity of the whole composite and prevent the possible detachment of Mn_3O_4 from the graphene sheets during cycling.

Supporting Information

TGA curves of rGO(18.8%)-Mn_3O_4 nanocomposite (composite 1), rGO(31.6%)-Mn_3O_4 nanocomposite (composite 2), rGO(45%)-Mn_3O_4 nanocomposite (composite 3), and bare Mn_3O_4 nanoparticles (Figure S1); Cyclic voltammograms of (a) rGO(18.8%)-Mn_3O_4 nanocomposite (composite 1), (b) rGO(45%)-Mn_3O_4 nanocomposite (composite 3), and (c) pure rGO at different scan rates in the voltage range from -0.1 V-0.8 V in 1 M Na_2SO_4 electrolyte (Figure S2); and TEM image of the rGO(31.6%)-Mn_3O_4 nanocomposite electrode after 1000 cycles (Figure S3).

Acknowledgments

This work was funded by an Australian Research Council (ARC) Discovery Project (DP1094261). The authors also would like to thank Dr. Tania Silver at the University of Wollongong for critical reading of the manuscript, as well as Mr. Darren Attard and Mr. Alfred Chidembo for their great contributions.

References

[1] J. R. Miller, P. Simon, Electrochemical capacitors for energy management. Science 321 (2008) 651.

[2] B. E. Conway, Electrochemical Supercapacitors: Scientific Fundamentals and Technological Applications, Kluwer, NY, 1999.

[3] P. Simon, Y. Gogotsi, Materials for electrochemical capacitors. Nature Materials 11 (2008) 845.

[4] E. Frackowiak, F. Beguin, Carbon materials for the electrochemical storage of energy in capacitors. Carbon 39 (2001) 937.

[5] X. Zhao, B. M. Sánchez, P. J. Dobson, P. S. Grant, The role of nanomaterials in redox-based supercapacitors for next generation energy storage devices. Nanoscale 3 (2011) 839.

[6] F. Fusalba, P. Gouérec, D. Villers, D. Belanger, Electrochemical characterization of polyaniline in nonaqueous electrolyte and its evaluation as electrode material for electrochemical supercapacitors. Journal of the Electrochemical Society 148 (2001) A1.

[7] Y. K. Zhou, B. L. He, W. J. Zhou, J. Huang, X. H. Li, B. Wu, H. L. Li, Electrochemical capacitance of well-coated single-walled carbon nanotube with polyaniline composites. Electrochimica Acta 49 (2004) 257.

[8] A. G. Pandolfo, A. F. Hollenkamp, Carbon properties and their role in supercapacitors. Journal of Power Sources 157 (2006) 11.

[9] L. L. Zhang and X. S. Zhao, Carbon-based materials as supercapacitor electrodes. Chemical Society Reviews 38 (2009) 2520.

[10] D. S. Su, R. Schlogl, Nanostructured carbon and carbon nanocomposites for electrochemical energy storage applications. ChemSusChem 3 (2010) 136.

[11] P. J. Hall, M. Mirzaeian, S. I. Fletcher, F. B. Sillars, A. J. R. Rennie, G. O. Shitta-Bey, G. Wilson, A. Cruden, R. Carter, Energy storage in electrochemical capacitors: designing functional materials to improve performance. Energy & Environmental Science 3 (2010) 1238.

[12] H. Wang, H. S. Casalongue, Y. Liang, H. Dai, $Ni(OH)_2$ nanoplates grown on graphene as advanced electrochemical pseudocapacitor materials. Journal of the American Chemical Society 132 (2010) 7472.

[13] S. Chen, J. Zhu, X. Wu, Q. Han, X. Wang, Graphene Oxide-MnO_2 Nanocomposites for Supercapacitors. ACS Nano 4 (2010) 2822.

[14] D. Wang, R. Kou, D. Choi, Z. Yang, Z. Nie, J. Li, L. V. Saraf, D. Hu, J. Zhang, G. L. Graff, J. Liu, M. A. Pope, I. A. Aksay, Ternary Self-Assembly of Ordered Metal Oxide–Graphene Nanocomposites for Electrochemical Energy Storage. ACS Nano 4 (2010) 1587.

[15] J. K. Lee, K. B. Smith, C. M. Hayner, H. H. Kung, Silicon nanoparticles-graphene paper composites for Li ion battery anodes. Chemical Communications 46 (2010) 2025.

[16] (a) Z. S. Wu, W. Ren, L. Wen, L. Gao, J. Zhao, Z. Chen, G. Zhou, F. Li, H. H. Cheng, Graphene anchored with Co_3O_4 nanoparticles as anode of lithium ion batteries with enhanced reversible capacity and cyclic performance. ACS Nano 4 (2010) 3187; (b) Z. Gao, J. Wang, Z. S. Li, W. L. Yang, B. Wang, M. J. Hou, Y. He, Q. Liu, T. Mann, P. P. Yang, M. L. Zhang, L. H. Liu, Graphene Nanosheet/Ni^{2+}/Al^{3+} Layered Double-Hydroxide Composite as a Novel Electrode for a Supercapacitor. Chemistry of Materials 23 (2011) 3509.

[17] (a) B. E. Conway, Transition from “supercapacitor” to “battery” behavior in electrochemical energy storage. Journal of Electrochemical Society 138 (1991) 1539; (b) J. P. Zheng, P. J. Cygan, T. R. Jow, Hydrous ruthenium oxide as an electrode material for electrochemical capacitors. Journal of Electrochemical Society 142 (1995) 2699.

[18] (a) W. L. Yang, Z. Gao, J. Wang, B. Wang, Q. Liu, Z. S. L, T. Mann, P. P. Yang, M. L. Zhang, L. H. Liu, Synthesis of reduced graphene nanosheet/urchin-like manganese dioxide composite and high performance as supercapacitor electrode. Electrochimica Acta, 69 (2012) 112; (b) X. Cui, F. Hu, W. Wer, W. Chen. Dense and long carbon nanotube arrays decorated with Mn_3O_4 nanoparticles for electrodes of electrochemical supercapacitors. Carbon 49

(2011) 1225; (c) M. Fang, X. Tan, M. Liu, S. Kang, X. Hu, L. Zhang, Low-temperature synthesis of Mn3O4 hollow-tetrakaidecahedrons and their application in electrochemical capacitors. CrystEngComm 13 (2011) 4915.

[19] A. A. Balandin, S. Ghosh, W. Z. Bao, I. Calizo, D. Teweldebrhan, F. Miao, C. N. Lau, Superior thermal conductivity of single-layer graphene. Nano Letters 8 (2008) 902.

[20] Z. S. Wu, W. C. Ren, L. B. Gao, J. P. Zhao, Z. P. Chen, B. L. Liu, D. M. Tang, B. Yu, C. B. Jiang, H. M. Cheng, Synthesis of graphene sheets with high electrical conductivity and good thermal stability by hydrogen arc discharge exfoliation. ACS Nano 3 (2009) 411.

[21] K. I. Bolotin, K. J. Sikes, Z. Jiang, M. Klima, G. Fudenberg, J. Hone, P. Kim, H. L. Stormer, Ultrahigh electron mobility in suspended graphene. Solid State Communications 146 (2008) 351.

[22] S. V. Morozov, K. S. Novoselov, M. I. Katsnelson, F. Schedin, D. C. Elias, J. A. Jaszczak, A. K. Geim, Giant intrinsic carrier mobilities in graphene and its bilayer. Physical Review Letters 100 (2008) 016602.

[23] D. A. Dikin, S. Stankovich, E. J. Zimney, R. D. Piner, G. H. B. Dommett, G. Evmenenko, S. T. Nguyen, R. S. Ruoff, Preparation and characterization of graphene oxide paper. Nature 448 (2007) 457.

[24] Y. H. Lin, T. Y. Wei, H. C. Chien, S. Y. Lu, Manganese Oxide/Carbon Aerogel Composite: an Outstanding Supercapacitor Electrode Material. Advanced Energy Materials 1 (2011) 901.

[25] (a) K. H. Seng, Z. P. Guo, Z. X. Chen, H. K. Liu, SnSb/graphene composite as anode materials for lithium ion batteries. Advanced Science Letters 4 (2011) 18; (b) C. F. Zhang, X. Peng, Z. P. Guo, C. B. Cai, Z. X. Chen, D. Wexler, S. Li, H. K. Liu, Carbon-coated SnO_2/graphene nanosheets as highly reversible anode materials for lithium ion batteries. Carbon 50 (2012) 1897; (c) G. D. Du, K. H. Seng, Z. P. Guo, RSC Advances 1 (2011) 690; (d) D. Li, M. Müller, S. Gilje, R. B. Kaner, G. G. Wallace, Processable aqueous dispersions of graphene nanosheets. Nature Nanotechnology 3 (2008) 101.

[26] A. Vázquez-Olmos, R. Redón, G. Rodríguez-Gattorno, M. Estherata-Zamora, F. Morales-Leal, A. L. Fernández-Osorio, J. M. Saniger, One-step synthesis of Mn_3O_4 nanoparticles: Structural and magnetic study. Journal of Colloid and Interface Science 291 (2005) 175.

[27] B. J. Li, H. Q. Cao, J. Shao, M. Z. Qu, J. H. Warner, Superparamagnetic Fe3O4 nanocrystals@graphene composites for energy storage devices. Journal of Materials Chemistry 21 (2011) 5069.

[28] T. Cassagneau, J. H. Fendler, S. A. Johnson, T. E. Mallouk, Self-Assembled Diode Junctions Prepared from a Ruthenium Tris(Bipyridyl) Polymer, n-Type TiO_2 Nanoparticles, and Graphite Oxide Sheets. Advanced Materials 12 (2000) 1363.

[29] H. L. Wang, L. F. Cui, Y. Yang, H. S. Casalongue, J. T. Robinson, Y. Y. Liang, Y. Cui, H. J. Dai, Mn_3O_4-Graphene Hybrid as a High-Capacity Anode Material for Lithium Ion Batteries. Journal of the American Chemical Society 132 (2010) 13978.

[30] Y. G. Wang, H. S. Zhou, To draw an air electrode of a Li-air battery by pencil. Energy & Environmental Science 4 (2011) 1704.

[31] Y. Zhou, Q. L. Bao, L. A. L. Tang, Y. L. Zhong, K. P. Loh, Hydrothermal dehydration for the "green" reduction of exfoliated graphene oxide to graphene and demonstration of tunable optical limiting properties. Chemistry of Materials. 21 (2009) 2950.

[32] A. Gupta, G. Chen, P. Joshi, S. Tadigadapa, P. C. Eklud, Raman scattering from high-frequency phonons in supported n-graphene layer films. Nano Letters 6 (2006) 2667.

[33] M. C. Bernard, A. Hugot-Le Goff, B. V. Thi, S. Cordoba de Torresi, Electrochromic Reactions in Manganese Oxides I. Raman Analysis. Journal of Electrochemical Society 140 (1993) 3065.

[34] C. M. Julien, M. Massot, C. Poinsignon, Lattice vibrations of manganese oxides: Part I. Periodic structures. Spectrochimica Acta A 60 (2004) 689.

[35] V. Srinivasan, J. W. Weidner, Studies on the capacitance of nickel oxide films: effect of heating temperature and electrolyte concentration. Journal of Electrochemical Society 147 (2000) 880.

[36] J. W. Long, A. L. Young, D. R. Rolison, Spectroelectrochemical characterization of nanostructured, mesoporous manganese oxide in aqueous electrolytes. Journal of Electrochemical Society 150 (2003) A1161.

[37] L. Li, Z. P. Guo, A. J. Du, H. K. Liu, Rapid microwave-assisted synthesis of Mn_3O_4-graphene nanocomposite and its lithium storage properties. Journal of Materials Chemistry 22 (2012) 3600.

[38] (a) B. Wang, J. Park, C. Y. Wang, H. Ahn, G. X. Wang, Mn_3O_4 nanoparticles embedded into graphene nanosheets: Preparation, characterization, and electrochemical properties for

supercapacitors. Electrochimica Acta 55 (2010) 6812; (b) M. Fang, X. L. Tan, M. Liu, S. H. Kang, X. Y. Hu, L. D. Zhang, Low-temperature synthesis of Mn_3O_4 hollow-tetrakaidecahedrons and their application in electrochemical capacitors. CrystEngComm 13 (2011) 4915; (c) X. W. Cui, F. P. Hu, W. F. Wei, W. X. Chen, Dense and long carbon nanotube arrays decorated with Mn_3O_4 nanoparticles for electrodes of electrochemical supercapacitors. Carbon 49 (2011) 1225.

[39] (a) K. W. Nama, K. B. Kim, Manganese oxide film electrodes prepared by electrostatic spray deposition for electrochemical capacitors. Journal of Electrochemical Society 153 (2006) A81-A88; (b) J. H. Kim, K. H. Lee, L. J. Overzet, G. S. Lee, Synthesis and Electrochemical Properties of Spin-Capable Carbon Nanotube Sheet/MnO_x Composites for High-Performance Energy Storage Devices. Nano Letters 11 (2011) 2611.

[40] M. Chigane, M. Ishikawa, Manganese oxide thin film preparation by potentiostatic electrolyses and electrochromism. Journal of the Electrochemical Society 147 (2000) 2246.

[41] J. F. Moulder, W. F. Strickle, P. E. Sobol, K. D. Bomben, Handbook of X-ray Photoelectron Spectroscopy, Perkin-Elmer Corporation: Physical Electronics Division: Eden Prairie, MN, 1992.

[42] D. Briggs, M. P. Seah, Practical Surface Analysis, 2nd ed., John Wiley & Sons, 1996.

[43] S. Komaba, T. Tsuchikawa, A. Ogata, N. Yabuuchi, D. Nakagawa, M. Tomita, Nano-structured birnessite prepared by electrochemical activation of manganese(III)-based oxides for aqueous supercapacitors. Electrochimica Acta 59 (2012) 455.

[44] J. W. Lee, A. S. Hall, J. D. Kim, T. E. Mallouk, A Facile and Template-Free Hydrothermal Synthesis of Mn_3O_4 Nanorods on Graphene Sheets for Supercapacitor Electrodes with Long Cycle Stability. Chemistry of Materials 24 (2012) 1158.

Supporting Information

Synthesis of Mn_3O_4-anchored graphene sheet nanocomposites via a facile, fast microwave hydrothermal method and their supercapacitive behavior

Li Li,[a] Kuok Hau Seng, [a] Huakun Liu, [a] Ivan P. Nevirkovets,[a] Zaiping Guo, [*,a, b]

a Institute for Superconducting and Electronics Materials, University of Wollongong, Wollongong 2519, Australia

b School of Mechanical, Materials, and Mechatronic Engineering, University of Wollongong, Wollongong 2522, Australia

Table of contents

Figure S1 TGA curves of rGO(18.8%)-Mn_3O_4 nanocomposite (composite 1) , rGO(31.6%)-Mn_3O_4 nanocomposite (composite 2), rGO(45%)-Mn_3O_4 nanocomposite (composite 3), and bare Mn_3O_4 nanoparticles.

Figure S2 Cyclic voltammograms of (a) rGO(18.8%)-Mn_3O_4 nanocomposite (composite 1), (b) rGO(45%)-Mn_3O_4 nanocomposite (composite 3), and (c) pure rGO at different scan rates in the voltage range from -0.1 V−0.8 V in 1 M Na_2SO_4 electrolyte.

Figure S3 TEM image of the rGO(31.6%)-Mn_3O_4 nanocomposite electrode after 1000 cycles. The red circle indicates an aggregation of MnO_x particles. Inset is the corresponding selected-area electron diffraction pattern.

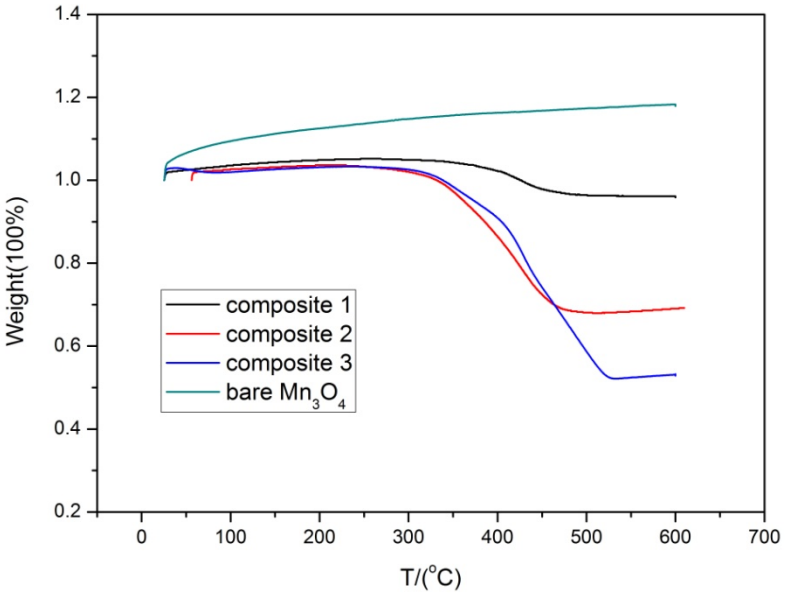
1.4
1.2
1.0
0.8
0.6
0.4
0.2
Weight(100%)
0
100
200
300
400
500
600
700
T/(°C)
composite 1
composite 2
composite 3
bare Mn3O4

Figure S1

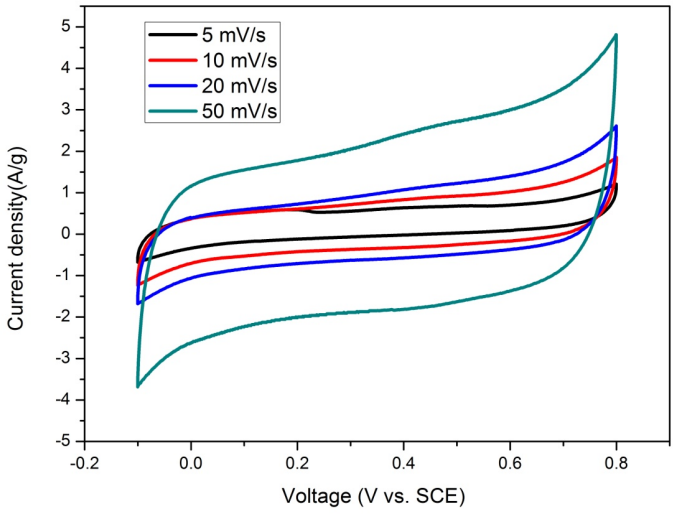
5 mV/s
10 mV/s
20 mV/s
50 mV/s
Current density(A/g)
Voltage (V vs. SCE)
5
4
3
2
1
0
-1
-2
-3
-4
-5
-0.2
0.0
0.2
0.4
0.6
0.8

Figure S2(a)

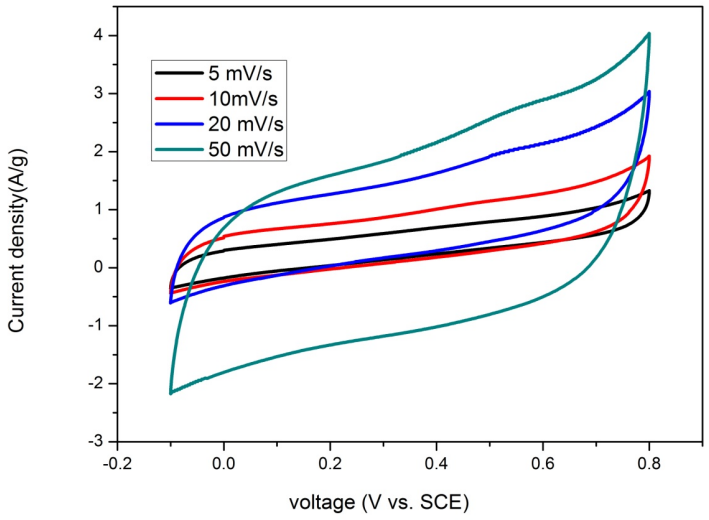
5 mV/s
10mV/s
20 mV/s
50 mV/s
Current density(A/g)
voltage (V vs. SCE)
4
3
2
1
0
-1
-2
-3
-0.2
0.0
0.2
0.4
0.6
0.8

Figure S2(b)

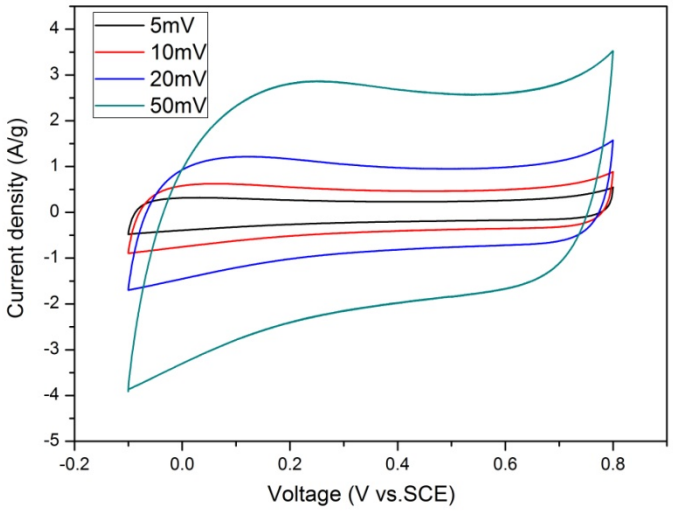
5mV
10mV
20mV
50mV
Current density (A/g)
Voltage (V vs.SCE)
4
3
2
1
0
-1
-2
-3
-4
-5
-0.2
0.0
0.2
0.4
0.6
0.8

Figure S2(c)

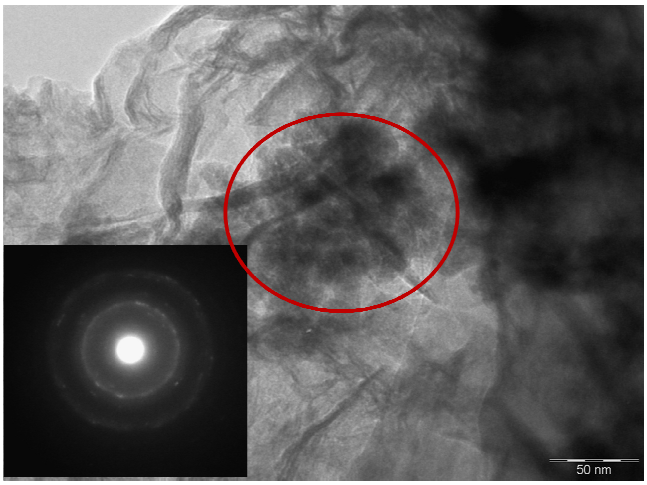

Figure S3

Table 1. Specific capacitance (F/g) of bare Mn_3O_4 nanoparticles and rGO(31.6%)-Mn_3O_4 composite at different scan rates at the first cycle.

	5 mV/s	10 mV/s	20 mV/s	50 mV/s
Bare Mn_3O_4	87	66	52	35
Composite	153	127	106	86